SIAM J. SCI. COMPUT.
Vol. 24, No. 6, pp. 1951–1973

VERLET-I/R-RESPA/IMPULSE IS LIMITED BY NONLINEAR INSTABILITIES*

QUN MA†, JESÚS A. IZAGUIRRE†, AND ROBERT D. SKEEL‡

Abstract. This paper shows that in molecular dynamics (MD) when constant- energy (NVE) simulations of Newton's equations of motion are attempted using the multiple time stepping (MTS) integrator Verlet-I/r-RESPA/Impulse, there are nonlinear instabilities when the longest step size is a third or possibly a fourth of the period(s) of the fastest motion(s) in the system. This is demonstrated both through a thorough set of computer experiments and through the analysis of a nonlinear model problem. The numerical experiments include not only the unconstrained dynamics simulation of a droplet of flexible water and a flexible protein, but also the constrained dynamics simulation of a solvated protein, representing a range of simulation protocols commonly in use by biomolecular modelers. The observed and predicted instabilities match exactly. Previous work has identified and explained a linear instability for Verlet-I/r-RESPA/Impulse at around half the period of the fastest motion. Mandziuk and Schlick discovered nonlinear resonances in single time stepping MD integrators, but unstable nonlinear resonances for MTS integrators are reported here for the first time. This paper also offers an explanation on the instability of MTS constrained molecular dynamics simulations of explicitly solvated proteins. More aggressive multiple step sizes are possible with mild Langevin coupling or targeted Langevin coupling, and its combination with the mollified Impulse method permits step sizes 3 to 4 times larger than Verlet-I/r-RESPA/Impulse while still retaining some accuracy.

Key words. long molecular dynamics simulations, Verlet-I/r-RESPA/Impulse, multiple time stepping, nonlinear instability, KAM theory, mollified Impulse method, Langevin stabilization

AMS subject classifications. 34D04, 65L05, 70F04, 70F08

PII. S1064827501399833

1. Introduction.

This paper uncovers additional stability limitations of multiple time stepping (MTS) integrators for molecular dynamics (MD) that attempt to bridge time scales. In particular, it is shown that when constant-energy (NVE) simulations of Newton's equations of motion are attempted using the MTS integrator Verlet-I [12]/r-RESPA [42]/Impulse, there are nonlinear instabilities when the longest step size is a third or possibly a fourth of the period(s) of the fastest motion(s) in the system. This is demonstrated both through a thorough set of computer experiments and through the analysis of a nonlinear model problem. The observed and predicted instabilities match exactly.

A linear instability for Verlet-I/r-RESPA/Impulse at around half the period of the fastest motion has been identified and explained by previous work [9, 40]. Mandziuk and Schlick [29] discovered nonlinear resonances in single time stepping MD integrators, but unstable nonlinear resonances for MTS integrators are reported here for the first time.

*Received by the editors December 19, 2001; accepted for publication (in revised form) November 18, 2002; published electronically May 6, 2003.
http://www.siam.org/journals/sisc/24-6/39983.html

†Department of Computer Science and Engineering, University of Notre Dame, Notre Dame, IN 46556-0309 (qma1@cse.nd.edu, izaguirr@cse.nd.edu). The work of these authors was supported in part by NSF grant BIOCOMPLEXITY-IBN-0083653, NSF CAREER award ACI-0135195, and a grant from the University of Notre Dame.

‡Department of Computer Science and Beckman Institute, University of Illinois, 1304 West Springfield Avenue, Urbana, IL 61801-2987 (skeel@cs.uiuc.edu). The work of this author was supported in part by NSF grants DMS-9971830, DBI-9974555 and NIH grant P41RR05969 and was initiated while visiting the Mathematics Department, University of California, San Diego.

We offer a two-part solution to enhance the stability of Verlet-I/r-RESPA/Impulse: the use of the *mollified Impulse* method [9, 20], a more stable variant of Verlet-I/r-RESPA/Impulse, along with the use of mild *Langevin coupling* [2, 15, 17] or *targeted Langevin coupling* [25]. This combination allows us to perform stable simulations with step sizes 3 to 4 times larger than Verlet-I/r-RESPA/Impulse while still retaining some accuracy.

1.1. Motivation. The modeling of large biological molecules is an area of great promise, with the availability of genomic information and protein crystal structures. Scientists want to compute dynamics and thermodynamic properties of these molecules to be able to predict drug affinity, etc. Molecular dynamics is the most widely used simulation technique for these calculations. Starting with the atomic coordinates, the molecular connectivity, and force field parameters, long trajectories are computed by solving Newton's equations of motion. A severe limitation in the ability of these simulations is given by the great range of time scales in biological systems, which span fifteen orders of magnitude.

1.2. Time scale limitations of molecular dynamics. Molecular dynamics solves the system of ODEs given by

$$\dot{\mathbf{q}} = \mathbf{M}^{-1}\mathbf{p}, \qquad \dot{\mathbf{p}} = -U'(\mathbf{q}), \tag{1.1}$$

where $\mathbf{q}$ is the position vector, $\mathbf{p}$ is the momentum vector, $U(\mathbf{q})$ is the potential energy, $-U'(\mathbf{q})$ is the force, and $\mathbf{M}$ is the mass matrix.

In an attempt to bridge the time scale gap between simulations and the phenomena of interest, multiple time stepping integrators have been introduced and have been an area of active research for more than a decade. The prototypical algorithm is the Verlet-I/r-RESPA/Impulse integrator, which splits the forces into fast and slow components and evaluates the former more frequently than the latter.

Assuming the fast force is harmonic, the discretization of this problem using Verlet-I/r-RESPA/Impulse with step size h for the slow part and analytical solution of the fast part is given by the following:

$\frac{1}{2}$ kick:

$$\mathbf{p}_0^+ = \mathbf{p} - \frac{h}{2}U'(\mathbf{q}). \tag{1.2}$$

oscillate: Let $s' = \sin h\Omega$ and $c' = \cos h\Omega$; we have

$$\begin{bmatrix} \mathbf{q}_1 \\ \mathbf{p}_{1/2}^+ \end{bmatrix} = \begin{bmatrix} c' & \frac{s'}{\Omega} \\ -\Omega s' & c' \end{bmatrix} \begin{bmatrix} \mathbf{q} \\ \mathbf{p}_0^+ \end{bmatrix}. \tag{1.3}$$

$\frac{1}{2}$ kick:

$$\mathbf{p}_1 = \mathbf{p}_{1/2}^+ - \frac{h}{2}U'(\mathbf{q}_1). \tag{1.4}$$

Verlet-I/r-RESPA/Impulse exhibits severe instability when the longest step size h is a multiple of the period of the fastest motion and a numerical instability at half the shortest period. These results have been confirmed through numerical experiments [8] and using simple linear-force model problems [2, 36, 40, 7].

1.3. Linear instabilities of multiple time stepping integrators. For explicitly solvated biological molecules and unconstrained MD simulations, the shortest period is around 10 fs and the linear instability occurs at about 5 fs. It turns out that some systematic drift can be observed in simulations reported in the literature even when using longest time steps around 3 or 4 fs; cf. Figure 2 in [8], Figure 3 in [44], and [14].

In an effort to overcome the linear instability of Verlet-I/r-RESPA/Impulse, we and other researchers have developed the mollified Impulse method (MOLLY) [9, 10, 16, 17, 18, 20]. MOLLY defines the slow part of the potential energy at time-averaged positions, and the force is made a gradient of the potential energy. The time average is obtained by doing dynamics over vibrations using forces that produce those vibrations. Thus,

$$U^{\text{slow}}(\mathbf{q}) \text{ becomes } U^{\text{slow}}(\mathcal{A}(\mathbf{q})), \tag{1.5}$$

with the force defined as a gradient of this averaged potential,

$$-\nabla U^{\text{slow}}(\mathbf{q}) \text{ is replaced by } -\mathcal{A}_{\mathbf{q}}(\mathbf{q})^{\mathrm{T}}\nabla U^{\text{slow}}(\mathbf{q}), \tag{1.6}$$

where $\mathcal{A}_{\mathbf{q}}(\mathbf{q})$ is a sparse Jacobian matrix.

This perturbation compensates for finite Δt artifacts. Intuitively, averaged positions are better than instantaneous values for a rapidly changing trajectory $\mathbf{q}(t)$. Perturbing the potential rather than the force ensures that the numerical integrator remains symplectic [37]. The force used by MOLLY is the gradient of the perturbed potential. The prefactor $\mathcal{A}_{\mathbf{q}}(\mathbf{q})^{\mathrm{T}}$ can be seen as a filter that eliminates components of the slow force Impulse in the directions of the fast forces, and thus improves the stability of Verlet-I/r-RESPA/Impulse. Different averaging functions give rise to MOLLY integrators with different stability and accuracy properties. We have used two different averaging methods, one based on explicit time averaging, which is reported in [40], and *Equilibrium* MOLLY, which in the case of linear forces is a nearly perfect filter[1] [20]. This method lengthens the longest step size by 50% and has been implemented in a production MD code, NAMD 2 [22], and in the experimental framework ProtoMol [19, 30].

1.4. Nonlinear instabilities in Verlet-I/r-RESPA/Impulse for unconstrained and constrained dynamics. The effect of nonlinear instabilities is a mild but systematic drift in the energy. This paper shows that there is a 3:1, and possibly a 4:1, nonlinear instability in Verlet-I/r-RESPA/Impulse for both unconstrained and constrained dynamics that significantly limits the stability region of the method. More precisely, there is a 3:1 unconditionally unstable resonance and a 4:1 conditionally stable resonance in Verlet-I/r-RESPA/Impulse.

We present empirical evidence of the nonlinear instabilities through precise computer experiments in section 2. Two sets of the flexible water simulations are performed: one under controlled conditions resembling the equilibrium point of the integrator, where the KAM stability theory holds, the other at room temperature. Both sets of experiments clearly reveal the 3:1 instability and the 4:1 resonance. One set of flexible protein simulations reveal the 3:1 instability that correlates to several fastest modes that are very close to each other.

[1] If all the fast forces are included in the averaging, then it is a perfect filter, although this is not the case in practice.

Even though with proper constraining using SHAKE [6, 43] or RATTLE [1, 31] the modes associated with stretching of bonds of polar hydrogen in the biomolecules and the bond stretching and angle bending in the solvent (water) molecules can be eliminated altogether, constrained dynamics simulations of explicitly solvated biomolecules using Verlet-I/r-RESPA/Impulse with SHAKE or RATTLE as the innermost integrator still exhibit instabilities when outer time steps are greater than 4 fs for long simulations. Simulations using Verlet-I/r-RESPA/Impulse with SHAKE as the innermost integrator suffer from the 4:1 and 3:1 nonlinear instabilities too.

We also perform a nonlinear analysis of Verlet-I/r-RESPA/Impulse applied to a simple nonlinear model problem. The analysis procedure is outlined in section 3. The application to multiple time stepping is in section 4. Appendix A justifies the analysis procedure.

Note that we may get instability even for longer step sizes than those with nonlinear resonances. This is due to the linear instability at half the period, which manifests itself in the neighborhood of that step size, and also to the fact that at nonzero temperatures different normal modes are mixed through energy transfer.

1.5. Removal of instabilities using mild stochasticity. The nonlinear instabilities of Verlet-I/r-RESPA/Impulse that are reported and analyzed in this paper are likely to be very significant in long MD simulations, which are made possible by the tenfold increase in computer power every five years and the desire to simulate longer processes that are of biological relevance and that can be experimentally verified, such as the folding of proteins. For applications of conformational dynamics where one wishes the energy to remain constant around a certain value of interest, the effect of nonlinear instabilities is also highly undesirable.

In our papers [17] we show the possibility of using very mild stochastic coupling to stabilize long step size integrators for Newtonian molecular dynamics. More specifically, stable and accurate integrations are obtained for coupling coefficients that are only a few percent of the natural decay rate of processes of interest, such as the velocity autocorrelation function. A 300% increase in the time step is possible using MOLLY with mild Langevin coupling while still computing dynamic properties accurately.

In our papers [25, 26] we show the possibility of using *targeted Langevin coupling,* a scheme that preserves linear momentum, to stabilize long step size integrators for Newtonian molecular dynamics. Even longer time steps are possible: A 400% increase in the time step has been achieved using MOLLY with targeted Langevin coupling while still computing dynamic properties accurately.

2. Numerical experiments. The numerical experiments in this section show that there are instabilities at around a third or possibly a fourth of the period(s) of the fastest motion(s) when integrating Newton's equations of motion using Verlet-I/r-RESPA/Impulse. All simulations use the CHARMM force field [27, 28]. The numerical experiments also show that for realistic biological systems such as explicitly solvated proteins, the step size is also limited by nonlinear instabilities even when the bonds of polar hydrogens in the proteins and the bonds and angles in waters are made rigid using the SHAKE or RATTLE algorithm. The justification of freezing the almost decoupled high frequency stretching can be found in [33].

Unstable resonances usually manifest themselves in the neighborhood of a certain step size: There is a definite range of step sizes that cause unbounded energy drift, even if the neighboring step sizes are stable. Examples of this resonance phenomenon are presented in [8].

KAM theory permits the analysis of nonlinear instabilities near an equilibrium point of an integrator [39, pp. 132–133]. For MTS integrators, equilibrium points are close to, but not exactly, the state at zero temperature. An example of empirical nonlinear instability analysis for the single time stepping integrator leapfrog is in [38]. Empirical nonlinear stability analysis for multiple time stepping is presented in this paper for the first time.

2.1. Model systems. We use three model systems (A, B, and C) for the simulations representing a range of simulation protocols in use by biomolecular modelers.

Model system A is a flexible TIP3P water system of 10 Å of radius, containing 423 atoms. The shortest period of this system is around 10 fs, corresponding to the symmetric and antisymmetric O-H bond stretching.

Model system B is a flexible protein system with Protein Data Bank (PDB) name 2mlt [11]. This system has two proteins, each containing 434 atoms. The shortest periods are about 9 fs, 10 fs, and 11 fs, which correspond to O-H, N-H, and C-H stretching, respectively.

Model system C is an explicitly solvated, rigid water/protein system: the 2mlt protein system (model system B) immersed in a box (about 58 Å× 38 Å× 25 Å) of rigid TIP3P water molecules. This system contains 5143 atoms. In the simulations of this system, the bonds of polar hydrogens in the protein, and the O-H bonds and H-O-H angles in waters are made rigid by using the SHAKE method. The periods of the remaining fastest modes are in the range of 18 to 24 fs, which correspond to the H-X-H angle bending (where X represents a nonhydrogen atom) and C=C stretching.

2.2. Power spectrum analysis for the model systems. All possible vibrations of a molecular system can be described as a superposition of fundamental oscillations, which are termed as *normal modes* for the molecules. Power spectrum analysis of the systems of interest forms the basis of correlating the time step related nonlinear instabilities with one or many of the normal modes.

We perform power spectrum analysis of the time history of the energy of the simulation to reveal the characteristic frequencies of the normal modes of the system. In order to make the best use of the power spectrum analysis result, we show the power spectra versus periods along with the step size related energy drift from the simulations in section 2.6; see the subfigure on the right of Figures 2.2, 2.4, and 2.5.

Wave-number unit is typically reported in the literatures, which is the number of waves per centimeter. The wave-numbers of the normal modes of the systems of interest are presented in Figure 2.1 for reference. All simulations used Verlet-I/r-RESPA/Impulse with an inner time step of 1 fs and outer time step of 2 fs and have a length of 200 ps.

Not surprisingly, the size of the inner time step of the MTS integrators used in the MD simulations affects the accuracy of the frequencies (and thus periods and wave-numbers) of the fastest motions. The frequencies and errors are shown in Table 2.1. The method of nonbonded force evaluation generally does not affect the accuracy of the frequencies of the fastest motions.

2.3. Measuring instabilities. We use the *"percent relative drift of total energy,"* D_{rel}, as a metric to measure the instabilities [20], which is given as follows:

$$D_{\text{rel}} = 100bL/K, \tag{2.1}$$

where b is the slope of the linear curve fit of the block-averaged total energy, L is the simulation length, and K is the average kinetic energy throughout the simulation.

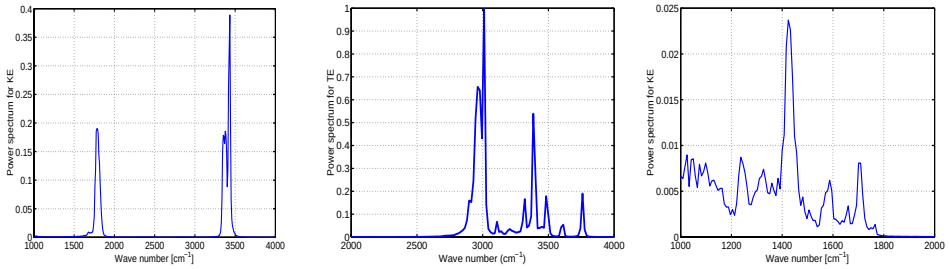

FIG. 2.1. *Characteristic frequencies of the fastest normal modes obtained from a* 200 *ps MD simulation of the flexible water system (on the left, including the symmetric and asymmetric bond stretching and angle bending), the flexible* 2*mlt protein system (on the middle, including the bond stretching of O-H, N-H, and C-H), and solvated* 2*mlt system constrained with SHAKE (on the right, including the angle bending of H-X-H, possibly bond stretching of C=C, and possibly some nonbonded interactions).*

TABLE 2.1

The periods for symmetric and asymmetric bond stretching in a droplet of flexible water. It is seen that the bigger the inner step size, the smaller the periods. The unit for the step sizes and periods is femtosecond (fs). Direct method is used for Coulomb force evaluation.

Integrator (Δt, δt)	Period	Error (%)
Impulse (2.0, 0.1)	(9.87, 10.07)	(−, −)
Impulse (2.0, 1.0)	(9.71, 9.91)	(1.63, 1.50)
Leapfrog (−, 2.0)	(9.12, 9.33)	(7.65, 7.35)

For a fixed simulation length, the bigger the value of D_{rel}, the more unstable the simulation becomes. In order to measure the goodness of the linear curve fit, we define the error bars as two times the *"percent relative root mean square deviation,"* δ_{rel}, which is given as follows:

$$\delta_{\text{rel}} = \frac{100}{K}\sqrt{\sum_{i=1}^{N}(y_i - \tilde{y}_i)^2/N}, \tag{2.2}$$

where N is the number of data points of the block-averaged total energy, y_i is the block-averaged total energy at block-averaged time t_i, $\tilde{y}_i$ is the value of the fitted straight line at t_i.

2.4. Simulation protocol. Each simulation of flexible waters has a length of 500 ps. The system was minimized using 10000 steps of conjugate-gradient minimization. Then the system was equilibrated for 100 ps. One system was equilibrated at 0.015 K and the other was equilibrated at 300 K.

Each simulation of flexible 2mlt proteins has a length of 10 ns. The system was minimized using 80000 steps of conjugate-gradient minimization. Then the system was equilibrated for 200 ps at 300 K.

Each simulation of the explicitly solvated 2mlt proteins system has a length of 500 ps. The bonds of polar hydrogens in the protein, the O-H bonds, and H-O-H angles in water are made rigid using the SHAKE method. The system was minimized using 30000 steps of conjugate-gradient minimization. Then the system was equilibrated for 200 ps at 300 K.

2.5. Simulation programs. We used the program NAMD2.3 [22] to minimize and equilibrate the flexible water system. Then we ran simulations of this system using ProtoMol, an experimental component-based framework for MD simulations [19, 30]. ProtoMol has a modular design that allows for easy prototyping of complex methods, and it is freely available at http://www.nd.edu/~lcls/Protomol.html.

For the protein and the solvated protein systems, we used the program NAMD2.5 to minimize and equilibrate them and used the same program for the actual simulation runs.

2.6. Numerical results. Numerical results on the step size–related, nonlinear instabilities are summarized here for all three model systems. In the interest of reproducibility of our results, we provide additional details to perform these simulations in Appendix B.

2.6.1. Flexible water at near zero temperature. We perform simulations of flexible water at 0.015 K. The instabilities associated with outer step sizes are plotted in Figure 2.2 in which each data point represents a 500 ps simulation. It is clear that in the neighborhood of $\Delta t = 3.33$ fs there is an unstable resonance (3:1) that manifests itself in an unmistakable drift at that step size. A milder resonance occurs at around $\Delta t = 2.57$ fs (4:1).

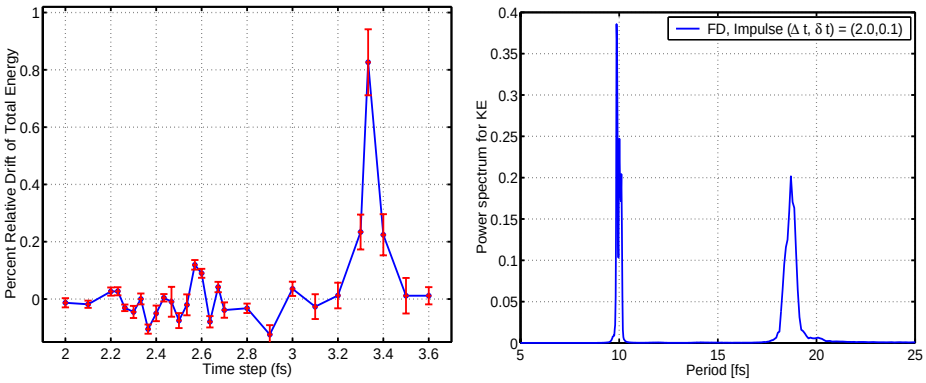

FIG. 2.2. *On the left: Energy drift for Verlet-I/r-RESPA/Impulse applied to a* 20*Å-diameter sphere of flexible water at about* 0.015 *K. Each point represents a* 500 *ps MD simulation with a step size* Δt *given by the x-axis and an innermost step size* δt *equal or very close to* 0.1 *fs so that the instabilities of the simulations are not due to the errors in the inner integrator; cf.* [5]. The peaks at step sizes of 2.57 fs and 3.33 fs show evidence of 4:1 resonance and 3:1 instability. *On the right: The periods of the fastest normal modes from a* 200 *ps simulation of the same system with inner time step of* 0.1 *fs (at* 300 *K).*

2.6.2. Flexible water at room temperature. We also explored whether or not the instability effect is present at room temperature using the same flexible water system equilibrated at 300 K. We are able to pinpoint the same instabilities as in the simulations near the equilibrium point. The results are shown in Figure 2.3.

2.6.3. Flexible 2mlt at room temperature. In addition to simulations of flexible waters, we perform simulations of the flexible 2mlt protein. The instabilities associated with outer step sizes are plotted in Figure 2.4 in which each data point represents a 10 ns simulation. Particle Mesh Ewald (PME) is used for Coulomb force evaluation [3, 4, 34, 45]. The results show that in the neighborhoods of $\Delta t = 3.00$,

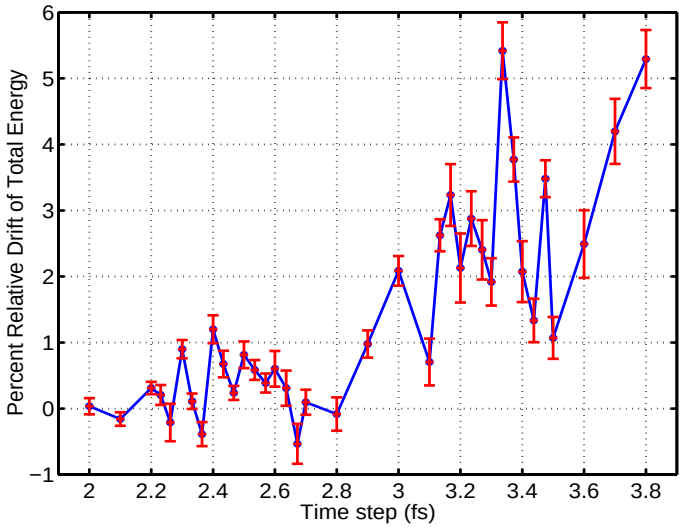

FIG. 2.3. *Same as in Figure* 2.2 *(subfigure on the left) except the temperature here is* 300 *K.* The peaks at step sizes of 2.40 fs and 3.33 fs show evidence of 4:1 resonance and 3:1 instability. *This figure also shows that we may get instability even for longer step sizes in the neighborhood of nonlinear resonances (the last few data points with* $3.33 < \Delta t \leq 3.80$ *(fs)). The normal modes plot for the same system is included in Figure* 2.2 *(on the right).*

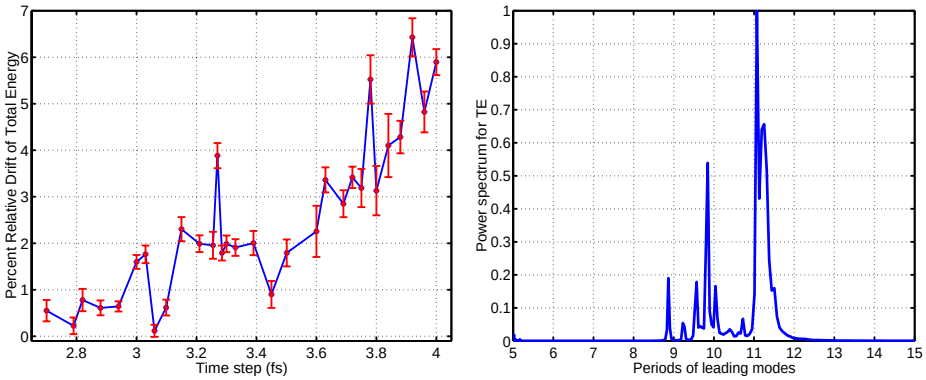

FIG. 2.4. *On the left: Energy drift for Verlet-I/r-RESPA/Impulse applied to a flexible protein, 2mlt, at* 300 *K. Each point represents a* 10 *ns MD simulation with a step size* Δt *given by the x-axis and an inner step size* δt *equal to* 1/3 *of outer step size. PME is used for Coulomb force evaluation.* The peaks at step sizes of $\Delta t = 3.00, 3.27, 3.78$ fs, show 3:1 instability. *On the right: The periods of the fastest normal modes from a* 200 *ps simulation of the same system with inner time step of* 1 *fs (at* 300 *K).*

3.27, and 3.78 fs, there are unstable resonances, which correspond to one third of the periods of O-H, N-H, and C-H stretching, respectively.

2.6.4. Rigid water/2mlt at room temperature. Finally, we performed simulations of the solvated 2mlt system where the bond lengths of all the bonds of polar hydrogen in the protein and the water molecules are constrained using SHAKE algorithm. The results are shown in Figure 2.5 in which each point represents a 500 ps simulation. PME is used for Coulomb force evaluation. Simulations with outer

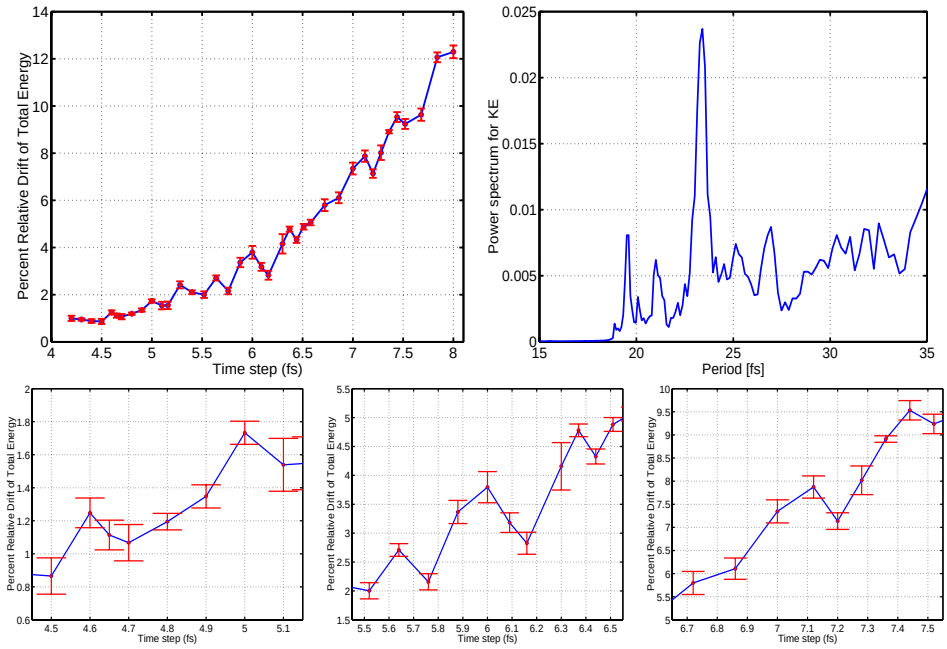

FIG. 2.5. *Upper left: Energy drift for Verlet-I/r-RESPA/Impulse applied to the explicitly solvated 2mlt system, at 300 K. Each point represents a 500 ps MD simulation with a step size Δt given by the x-axis and an inner step size δt in the range of 0.82 to 1 fs. Upper right: The periods of the fastest normal modes from a 200 ps simulation of the same system with inner time step of 1 fs (at 300 K). Lower left, lower middle, and lower right are the zoom-ins of the plot on the upper left. The bonds of polar hydrogens in the protein, the O-H bonds and H-O-H angles in water are made rigid using the SHAKE method. It is hard to make any specific identifications of nonlinear resonance just from these figures because the remaining modes are continuous. Most likely these drifts correspond to the combined effects of 4:1 and 3:1 resonances.*

time step greater than 4 fs are unstable. It is hard to make any specific identifications of nonlinear resonance just from these figures because the remaining modes are continuous. Most likely these drifts correspond to the combined effects of 4:1 and 3:1 resonances associated with the remaining modes including angle bending, C=C stretching, and some of the nonbonded interactions.

Note that simulations may become unstable even for step sizes larger than the ones that just excite the nonlinear instabilities. Examples include the last few data points in Figure 2.3 with $3.3363 < \Delta t \leq 3.8$ (fs) and the last few data points in Figure 2.4 with $\Delta t > 3.8$ fs.

3. Analysis procedure. Given here is a procedure for analyzing the stability of a reversible symplectic map, which extends the analysis of [35].

3.1. Assumptions. Let $y_{n+1} = M(y_n)$ be the map of interest. In the present context M depends on a step size parameter h, so we may at times write $M_h(y)$ instead of $M(y)$. Reversible means that $RM(RM(y)) = y$, where $R = \mathrm{diag}(1, -1)$. Most practical reversible symplectic integrators, including simple implicit ones [41], can be expressed

$$M(y) = RN^{-1}(RN(y)), \tag{3.1}$$

where $N(y) = N_{h/2}(y)$ is itself an area-preserving map.[2] It is easily verified that $M(y)$ is indeed reversible. Given here are the stability conditions for this important special case of reversible maps *in terms of the simpler map* $N(y)$.

The analysis is valid only in some neighborhood of a fixed point $y^* = M(y^*)$ of the map. We assume that the Jacobian matrix $M'(y^*)$ is power-bounded, which is necessary for stability. Also assume that $y^* = (q^*, 0)$, which will be the case except possibly for values of h so large so as not to be of practical interest (see Appendix A, Proposition A.1).

3.2. Procedure.

Step 1. Express

$$N(y) = N(y^*) + \begin{bmatrix} a_{11} & a_{12} \\ -a_{21} & a_{22} \end{bmatrix} (y - y^*) + O(\|y - y^*\|^2). \tag{3.2}$$

For stability it is necessary that either $0 < a_{11}a_{22} < 1$ or $a_{11} = a_{22} = 0$ or $a_{12} = a_{21} = 0$ (see Appendix A, Proposition A.2). The symplectic property implies that the determinant $a_{11}a_{22} + a_{12}a_{21} = 1$.

Step 2. Choose $\alpha \neq 0$, $\beta \neq 0$ so that the map

$$N_{\mathrm{Y}}(Y) = \mathrm{diag}(\alpha, 1/\alpha)\,(N(y^* + \mathrm{diag}(\beta, 1/\beta)Y) - N(y^*)) \tag{3.3}$$

satisfies

$$N_{\mathrm{Y}}(Y) = \begin{bmatrix} \gamma & \sigma \\ -\sigma & \gamma \end{bmatrix} Y + O(\|Y\|^2), \tag{3.4}$$

where $\sigma^2 + \gamma^2 = 1$. This can be done as follows (see Appendix A, Proposition A.3):

$$\alpha = \left(\frac{a_{21}a_{22}}{a_{11}a_{12}}\right)^{1/4}, \qquad \beta = \left(\frac{a_{12}a_{22}}{a_{11}a_{21}}\right)^{1/4} \qquad \text{if } 0 < a_{11}a_{22} < 1, \tag{3.5}$$

$$\alpha = \left(\frac{a_{21}}{a_{12}}\right)^{1/2} \beta \qquad \text{if } a_{11} = a_{22} = 0, \tag{3.6}$$

$$\alpha = \left(\frac{a_{22}}{a_{11}}\right)^{1/2} \frac{1}{\beta} \qquad \text{if } a_{12} = a_{21} = 0. \tag{3.7}$$

Step 3. Express the map $N_{\mathrm{Y}}(Q, P)$ in complex form as

$$N_{\mathrm{z}}(z, \bar{z}) = \mu z + \mathrm{i}\mu r(z, \bar{z}), \tag{3.8}$$

where $z = Q + \mathrm{i}P$, $\mu = \gamma - \mathrm{i}\sigma$, and

$$r(z, \bar{z}) = c_1 z^2 + 2\bar{c}_1 z\bar{z} + c_2 \bar{z}^2 + c_3 z^2 \bar{z} + c_4 \bar{z}^3 + \mathrm{UTs}. \tag{3.9}$$

The UTs (unimportant terms) are defined to be the z^3 term, the $z\bar{z}^2$ term, and those of degree 4 or more. This can always be done (see Appendix A, Proposition A.4). Express $c_j = a_j + \mathrm{i}b_j$, where a_j and b_j are real, and define

$$a = 2a_1, \tag{3.10}$$

$$c = 2a_2, \tag{3.11}$$

$$f = 2a_3 - 12a_1b_1 + 4a_2b_2, \tag{3.12}$$

$$g = 2a_4 + 4a_2b_1 + 4a_1b_2. \tag{3.13}$$

[2] For conventional methods the momentum reversal $RN_{h/2}(Ry)$ is identical to the time reversal $N_{-h/2}(y)$ and hence $RN_{h/2}^{-1}(Ry)$ is the same as the *adjoint*, $N_{-h/2}^{-1}(y)$ [13].

Conclusion. (See Appendix A for proof.) Let $\lambda = \mu^2$.

1. *Third order resonance.* Suppose $\lambda^3 = 1$ but $\lambda \neq 1$. The map is stable at equilibrium if $c = 0$ and $-\sigma f - 3\gamma a^2 \neq 0$, and it is unstable if $c \neq 0$. Hence, third order resonance is normally unstable.
2. Suppose $\lambda^3 \neq 1$. Let

$$F = -\sigma(4\gamma^2 - 1)f - 3\gamma(4\gamma^2 - 1)a^2 - \gamma(4\gamma^2 - 3)c^2, \tag{3.14}$$

$$G = -\sigma(4\gamma^2 - 1)g + 2\gamma ac. \tag{3.15}$$

   (a) *Fourth order resonance.* Suppose $\lambda^4 = 1$. The map is stable at equilibrium if $|G| < |F|$, and it is unstable if $|G| > |F|$.
   (b) Suppose $\lambda^4 \neq 1$. The map is stable at equilibrium if $F \neq 0$.

4. Application to multiple time stepping. We apply the analysis procedure just outlined to a nonlinear model problem to obtain the nonlinear stability conditions on multiple time stepping algorithms.

4.1. The map. Assume a nonlinear model problem with potential energy given by

$$U(q) = \underbrace{\frac{1}{2}\Omega^2 q^2}_{\text{oscillate}} \underbrace{+\frac{1}{2}Aq^2 + \frac{1}{3}Bq^3 + \frac{1}{4}Cq^4}_{\text{kick}} + O(q^5), \tag{4.1}$$

where the splitting between the oscillate and kick step for Verlet-I/r-RESPA/Impulse is done as indicated.

The discretization of this problem using the first half of Verlet-I/r-RESPA/Impulse is given by the following:

$\frac{1}{2}$ kick:

$$p_0^+ = p - \frac{h}{2}(Aq + Bq^2 + Cq^3) + O(q^4). \tag{4.2}$$

$\frac{1}{2}$ oscillate: Let $s' = \sin\frac{h\Omega}{2}$ and $c' = \cos\frac{h\Omega}{2}$; we have

$$\begin{bmatrix} q_{1/2} \\ p_{1/2} \end{bmatrix} = \begin{bmatrix} c' & \frac{s'}{\Omega} \\ -\Omega s' & c' \end{bmatrix} \begin{bmatrix} q \\ p_0^+ \end{bmatrix}. \tag{4.3}$$

4.2. Main result. Let $\lambda = \mu^2$, where $\mu = \gamma - \mathrm{i}\sigma$ in which

$$\gamma = \begin{cases} \left(1 - \frac{h}{2}\frac{s'}{\Omega c'}A\right)^{1/2} c', & c' \neq 0, \\ 0, & c' = 0, \end{cases}$$

and

$$\sigma = \begin{cases} \left(1 + \frac{h}{2}\frac{c'}{\Omega s'}A\right)^{1/2} s', & \frac{s'}{\Omega} \neq 0, \\ 0, & \frac{s'}{\Omega} = 0. \end{cases}$$

We assume that either $-(s')^2 < \frac{hs'c'}{2\Omega}A < (c')^2$, or $\frac{s'}{\Omega} = A = 0$ or $c' = A = 0$. These assumptions are necessary to avoid linear instability at half the shortest period; cf. [40].

Applying the nonlinear instability analysis of section 3 we obtain the following nonlinear stability conditions:

1. Third order resonance. Suppose $\lambda^3 = 1$ but $\lambda \neq 1$. The map is stable at equilibrium if $B = 0$ and $C \neq 0$, and it is *unstable if* $B \neq 0$. This condition for stability is as stringent for MTS as it is for leapfrog, and thus Verlet-I/r-RESPA/Impulse is unstable in practice. This instability is confirmed by the numerical results in section 2.
2. Fourth order resonance. Suppose $\lambda = \mathrm{e}^{-\mathrm{i}\pi/2}$. The map is stable at equilibrium if $C < 0$ or $C > 2hB^2s'c'/\Omega$. It is unstable if $0 < C < 2hB^2s'c'/\Omega$. Thus, Verlet-I/r-RESPA/Impulse may or may not be stable at the fourth order resonance. This fourth order resonance is observed in our numerical experiments, although our experiments are not conclusive regarding whether this is an unstable nonlinear resonance.

4.3. Discussion. The case $\Omega \to 0$ and $A = \omega^2$ gives the leapfrog result

$$C > \frac{2}{\omega^2}B^2. \tag{4.4}$$

To assess the implication of the stability condition for 4:1 resonance, consider two particles separated by a distance r for which the fast force is harmonic and the slow force is electrostatic:

$$U(r) = \frac{1}{2}\Omega^2(r - r_0)^2 + kr^{-1}. \tag{4.5}$$

Assume $r_0 > 0$ and that there is a stable equilibrium at $r = r_* > 0$. Writing $r = r_* + q$, we have

$$U(r_* + q) = U(r_*) + \frac{1}{2}\Omega^2 q^2 + kr_*^{-3}q^2 - kr_*^{-4}q^3 + kr_*^{-5}q^4 + O(q^5), \tag{4.6}$$

which yields

$$A = 2kr_*^{-3}, \quad B = -3kr_*^{-4}, \quad C = 4kr_*^{-5}. \tag{4.7}$$

The condition given for stability becomes

$$k < 0 \quad \text{or} \quad h^2k^2r_*^{-3}\frac{\sin h\Omega}{h\Omega} < \frac{4}{9}k, \tag{4.8}$$

and the above condition is satisfied if

$$h^2kr_*^{-3} < \frac{4}{9}. \tag{4.9}$$

This relation can be interpreted in terms of the error due to the finite step size h used to sample the slow force. From [24, eq. (10)] it follows that discretization introduces an error $\frac{1}{24}h^2(-kr_*^{-2})^2$ in the potential energy, and comparing this to the potential energy kr_*^{-1} itself we get the quantity $estRelErr = \frac{1}{24}h^2kr_*^{-3}$. With this definition the condition for stability can be expressed

$$estRelErr < \frac{1}{54}, \tag{4.10}$$

which is satisfied either if the two particles are oppositely charged or if cutoffs are being chosen to yield reasonable accuracy. Neglected is the fact that in simulations of liquids, where particles can move closer together, the slow potential is defined as the product of the actual potential times times a switching function. The stability condition for 4:1 resonance is not satisfied for typical switching functions.

4.4. Proof of main result.

Step 1. (4.3) can be rewritten as

$$\begin{bmatrix} q_{1/2} \\ p_{1/2} \end{bmatrix} = \begin{bmatrix} c' - \frac{h}{2}\frac{s'}{\Omega}A & \frac{s'}{\Omega} \\ -\Omega s' - \frac{h}{2}c'A & c' \end{bmatrix} \left(\begin{bmatrix} q \\ p \end{bmatrix} - \frac{h}{2} \begin{bmatrix} 0 \\ 1 \end{bmatrix} (Bq^2 + Cq^3) \right) + O(q^4). \tag{4.11}$$

The elements of the matrix determine the linear stability condition stated in the result.

Step 2. In the case of $-(s')^2 < \frac{hs'c'}{2\Omega}A < (c')^2$,

$$\alpha = \left(\frac{(\Omega s' + \frac{h}{2}c'A)c'}{(c' - \frac{h}{2}\frac{s'}{\Omega}A)\frac{s'}{\Omega}} \right)^{1/4}, \tag{4.12}$$

$$\beta = \left(\frac{\frac{s'}{\Omega}c'}{(c' - \frac{h}{2}\frac{s'}{\Omega}A)(\Omega s' + \frac{h}{2}c'A)} \right)^{1/4}. \tag{4.13}$$

In the case of $\frac{s'}{\Omega} = A = 0$ or $c' = A = 0$,

$$\alpha = \Omega^{1/2}, \qquad \beta = \Omega^{-1/2}. \tag{4.14}$$

With these definitions α and β have removable singularities as functions of h when $A = 0$. From (3.2)–(3.4) and (4.12)–(4.14) we calculate

$$\gamma = \begin{cases} \left(1 - \frac{h}{2}\frac{s'}{\Omega c'}A\right)^{1/2} c', & c' \neq 0, \\ 0, & c' = 0, \end{cases} \tag{4.15}$$

and

$$\sigma = \begin{cases} \left(1 + \frac{h}{2}\frac{c'}{\Omega s'}A\right)^{1/2} s', & \frac{s'}{\Omega} \neq 0, \\ 0, & \frac{s'}{\Omega} = 0. \end{cases} \tag{4.16}$$

From (3.2)–(3.4) and (4.11), we get

$$\begin{bmatrix} Q_{1/2} \\ P_{1/2} \end{bmatrix} = \begin{bmatrix} \gamma & \sigma \\ -\sigma & \gamma \end{bmatrix} \left(\begin{bmatrix} Q \\ P \end{bmatrix} - \frac{h}{2} \begin{bmatrix} 0 \\ \beta \end{bmatrix} (\beta^2 BQ^2 + \beta^3 CQ^3) \right) + O(Q^4). \tag{4.17}$$

Step 3. With $\mu = \gamma - \mathrm{i}\sigma$ and $z = Q + \mathrm{i}P$, we have

$$Q = \frac{1}{2}(z + \bar{z}). \tag{4.18}$$

and

$$z_{1/2} = \mu\,(z - \mathrm{i}h\phi(z, \bar{z})) + \mathrm{UTs}, \tag{4.19}$$

where

$$\phi(z, \bar{z}) = \frac{\beta^3}{8}Bz^2 + \frac{\beta^3}{4}Bz\bar{z} + \frac{\beta^3}{8}B\bar{z}^2 + \frac{3\beta^4}{16}Cz^2\bar{z} + \frac{\beta^4}{16}C\bar{z}^3, \tag{4.20}$$

whence

$$c_1 = -\frac{h}{8}\beta^3 B, \quad c_2 = -\frac{h}{8}\beta^3 B, \quad c_3 = -\frac{3h}{16}\beta^4 C, \quad c_4 = -\frac{h}{16}\beta^4 C, \tag{4.21}$$

and

$$a = -\frac{h}{4}\beta^3 B, \quad c = -\frac{h}{4}\beta^3 B, \quad f = -\frac{3h}{8}\beta^4 C, \quad g = -\frac{h}{8}\beta^4 C. \tag{4.22}$$

Conclusions. Letting $\lambda = \mu^2$ and performing analyses for the cases $\lambda^3 = 1$ and $\lambda^3 \neq 1$, we obtain the main result. Note that with regard to the fourth order resonance, considering only the case where $\lambda = \mathrm{e}^{-\mathrm{i}\pi/2}$, for which $\sigma = \gamma = \sqrt{2}/2$, stability of the map at equilibrium requires $|C + h\beta^2 B^2| < |3C - h\beta^2 B^2|$, where $\beta^2 = \frac{s'c'}{\Omega\sigma\gamma}$.

For the case $\lambda^3 \neq 1$ and $\lambda^4 \neq 1$, the map is stable at equilibrium if $F \neq 0$, where

$$F = \frac{1}{8}h\beta^4 \left(3\sigma(4\gamma^2 - 1)C - \gamma(8\gamma^2 - 3)h\beta^2 B^2\right). \tag{4.23}$$

5. Discussion. In protein simulations, there are possibly several other factors that may also contribute to instability. Examples include difficulties in matching the cutoff radii for the short-/intermediate-/long-range forces for Coulomb interactions in Ewald splitting [3, 4, 45, 34] and group switching functions, e.g., when the group radii (intermediate or long) matches a critical distance between two neighboring groups and many others related to the arbitrary potential breakup [32]. Nonetheless, the step size–related nonlinear instabilities should not be neglected. In particular, although 4:1 nonlinear instability could be eliminated by designing a switching function that satisfies the inequality equation (4.9), 3:1 nonlinear instability is a general phenomenon. In some applications, accuracy limits the time step, but in the important cases shown here, the time step is limited by stability.

Appendix A. Justification of analysis procedure. This is a simplification of stability conditions in [35] for the case

$$M_h(y) = RN_{h/2}^{-1}(RN_{h/2}(y)), \tag{A.1}$$

where $N(y) = N_{h/2}(y)$ is itself an area-preserving map.

Proposition A.1. *Assume y_h^* can be obtained uniquely by analytical continuation from $y_0^* = (q_0^*, 0)$. Then $p_h^* = 0$.*

Proof. We show that Ry_δ^* is also a fixed point for $0 \leq \delta \leq h$. Since y_δ^* is a fixed point of the map M_δ, we have

$$y_\delta^* = RN_\delta{}^{-1}(RN_\delta(y_\delta^*)). \tag{A.2}$$

Multiplying both sides by R and then applying the map N_δ, we have

$$N_\delta(Ry_\delta^*) = RN_\delta(y_\delta^*), \tag{A.3}$$

following which we have

$$M_\delta(Ry_\delta^*) = RN_\delta{}^{-1}(RN_\delta(Ry_\delta^*)) = Ry_\delta^*. \tag{A.4}$$

Since $Ry_0^* = y_0^*$ and y_δ^* does not bifurcate for $0 \leq \delta \leq h$, we have

$$Ry_\delta^* \equiv y_\delta^*, \tag{A.5}$$

which implies $p_\delta^* \equiv 0$. ∎

Note that analytical continuation can be done for $\delta > 0$ as long as $M'_\delta(y_\delta^*) \neq I$, assuming consistency of M_δ, $U'(q_0^*) = 0$, and $U''(q_0^*) > 0$, where U refers to the potential energy as given by (4.1).

PROPOSITION A.2. *Let* $N'(y^*) = \left[\begin{smallmatrix} a_{11} & a_{12} \\ -a_{21} & a_{22} \end{smallmatrix}\right]$ *be the Jacobian matrix of the map* N *at the fixed point* y^*. *For stability of* M_h, *it is necessary that either* $0 < a_{11}a_{22} < 1$ *or* $a_{11} = a_{22} = 0$ *or* $a_{12} = a_{21} = 0$.

Proof. Multiplying both sides of (A.1) by R and then applying the map N, we have

$$N(RM_h(y)) = RN(y). \tag{A.6}$$

Forming the Jacobian matrix on both sides at the fixed point y^*, we have

$$N'(Ry^*)RM'(y^*) = RN'(y^*), \tag{A.7}$$

which leads to

$$M'(y^*) = RN'(y^*)^{-1}RN'(y^*). \tag{A.8}$$

The symplecticness property of N implies $a_{11}a_{22} + a_{12}a_{21} = 1$. The inverse of the Jacobian is given by

$$N'(y^*)^{-1} = \begin{bmatrix} a_{22} & -a_{12} \\ a_{21} & a_{11} \end{bmatrix}. \tag{A.9}$$

Thus, we have

$$M'_h(y^*) = \begin{bmatrix} a_{11}a_{22} - a_{12}a_{21} & 2a_{12}a_{22} \\ -2a_{11}a_{21} & a_{11}a_{22} - a_{12}a_{21} \end{bmatrix}. \tag{A.10}$$

Because $M'(y^*)$ is power bounded and $\det M'(y^*) = 1$, it has two eigenvalues λ, $\bar{\lambda}$ of unit modulus[3] and hence $|\mathrm{trace}(M'(y^*))| \leq 2$. If the trace is less than 2 in magnitude, then $0 < a_{12}a_{21} < 1$. If its magnitude is 2, then power-boundedness implies that the off-diagonal elements of $M'(y^*)$ are both zero, which further implies that $a_{11} = a_{22} = 0$ or $a_{12} = a_{21} = 0$. ∎

PROPOSITION A.3. *Let*

$$N_{\mathrm{Y}}(Y) = D_1(N(y^* + D_2Y) - N(y^*)), \tag{A.11}$$

where $D_1 = \mathrm{diag}(\alpha, 1/\alpha)$ *and* $D_2 = \mathrm{diag}(\beta, 1/\beta)$. *We can choose* D_1 *and* D_2 *so that* $N'_{\mathrm{Y}}(0)$ *is a rotation matrix and so that* $M_{\mathrm{Y}}(Y) = RN_{\mathrm{Y}}^{-1}(RN_{\mathrm{Y}}(Y))$ *is stable at* $Y = 0$ *if and only if* $M(y)$ *is stable at* $y = y_h^*$.

Proof. First,

$$y^* = RN^{-1}(RN(y^*)), \tag{A.12}$$

which implies

$$N(Ry^*) = RN(y^*). \tag{A.13}$$

[3]The eigenvalues of $M'(y^*)$ are $\lambda_{1,2} = a_{11}a_{22} - a_{12}a_{21} \pm 2\mathrm{i}\sqrt{a_{11}a_{12}a_{21}a_{22}}$.

Hence, since $y^* = (q^*, 0)$, we have

$$RN(y^*) = N(Ry^*) = N(y^*). \tag{A.14}$$

Multiplying both sides of (A.11) by D_1^{-1}, we have

$$N(y^* + D_2 Y) = {D_1}^{-1} N_{\mathrm{Y}}(Y) + N(y^*). \tag{A.15}$$

From the above we have

$$Y = {D_2}^{-1}(N^{-1}({D_1}^{-1} N_{\mathrm{Y}}(Y) + N(y^*)) - y^*), \tag{A.16}$$

which implies that the inverse of the map $N_{\mathrm{Y}}(Y)$ is given by

$${N_{\mathrm{Y}}}^{-1}(Y) = {D_2}^{-1}(N^{-1}({D_1}^{-1} Y + N(y^*)) - y^*). \tag{A.17}$$

Then

$$\begin{aligned} M_{\mathrm{Y}}(Y) &= RN_{\mathrm{Y}}^{-1}(RN_{\mathrm{Y}}(Y)) \\ &= RD_2^{-1}(N^{-1}(\underbrace{D_1^{-1}(RD_1}_{cancel}(N(y^* + D_2 Y) \underbrace{-N(y^*))) + N(y^*)}_{cancel}) - y^*). \end{aligned} \tag{A.18}$$

Because $D_1^{-1} R D_2^{-1} = R$ and (A.14), this becomes

$$M_{\mathrm{Y}}(Y) = RD_2^{-1}(N^{-1}(RN(y^* + D_2 Y)) - y^*) \tag{A.19}$$

or

$$M_{\mathrm{Y}}(Y) = D_2^{-1} M(y^* + D_2 Y) - y^*, \tag{A.20}$$

which is a symplectic transformation, $y = y^* + D_2 Y$, of the map M. A symplectic transformation preserves the stability property. Finally

$$N'_{\mathrm{Y}}(0) = D_1 N'(y^*) D_2, \tag{A.21}$$

which can be verified to be a rotation matrix. ∎

PROPOSITION A.4. *Let*

$$N_{\mathrm{Y}}(Y) = \begin{bmatrix} \gamma & \sigma \\ -\sigma & \gamma \end{bmatrix} Y + O(\|Y\|^2) \tag{A.22}$$

be symplectic. Let $z = Q + \mathrm{i}P$, and let $\mu = \gamma - \mathrm{i}\sigma$. Then the map becomes

$$z \mapsto N_z(z, \bar{z}) \stackrel{\mathrm{def}}{=} \mu z + \mathrm{i}\mu r(z, \bar{z}), \tag{A.23}$$

where

$$r(z, \bar{z}) = c_1 z^2 + 2\bar{c}_1 z\bar{z} + c_2 \bar{z}^2 + c_3 z^2 \bar{z} + c_4 \bar{z}^3 + \mathrm{UTs}. \tag{A.24}$$

Proof. See [35, eq. (2.15)]. ∎

Proof of conclusion. Perform a symplectic change of variables $X = N_{\mathrm{Y}}(Y)$ and the map becomes

$$X \mapsto M_{\mathrm{X}}(X) \stackrel{\mathrm{def}}{=} N_{\mathrm{Y}}(RN_{\mathrm{Y}}^{-1}(RY)), \tag{A.25}$$

which can be expressed as $X_1 = M_{\mathrm{X}}(X_0)$, where

$$X_1 = N_{\mathrm{Y}}(X_{1/2}), \qquad X_0 = RN_{\mathrm{Y}}(RX_{1/2}). \tag{A.26}$$

The new map M_{X} has the same stability properties at the origin as the map M_{Y}, and it is also reversible. It is expressed in complex form as

$$z_1 = N_{\mathrm{z}}(z, \bar{z}), \qquad z_0 = \overline{N_{\mathrm{z}}(\bar{z}, z)} = \bar{N}_{\mathrm{z}}(z, \bar{z}), \tag{A.27}$$

where $\bar{N}_{\mathrm{z}}$ is N_{z} with its coefficients complex conjugated. The map M_{X} satisfies the hypotheses of Lemma 4.2 of [35] with $\lambda = \mathrm{e}^{\mathrm{i}\phi} = \mu^2$, so its complex equivalent has the form

$$z_1 = \mu^2 z_0 + \mathrm{i}\mu L(\mu z_0, \bar{\mu}\bar{z_0}), \tag{A.28}$$

where

$$L(z, \bar{z}) = az^2 + 2az\bar{z} + c\bar{z}^2 + (f + \mathrm{i}(a^2 - c^2))z^2\bar{z} + g\bar{z}^3 + \mathrm{UTs} \tag{A.29}$$

and a, c, f, g are real. Substituting (A.27) into (A.28) gives

$$N_{\mathrm{z}}(z, \bar{z}) = \mu^2 \bar{N}_{\mathrm{z}}(z, \bar{z}) + \mathrm{i}\mu L(\mu \bar{N}_{\mathrm{z}}(z, \bar{z}), \bar{\mu} N_{\mathrm{z}}(\bar{z}, z)). \tag{A.30}$$

From (A.23), we have

$$\bar{N}_{\mathrm{z}}(z, \bar{z}) = \bar{\mu} z - \mathrm{i}\bar{\mu}\bar{r}(z, \bar{z}), \tag{A.31}$$

and substituting both equations into (A.30) gives

$$r(z, \bar{z}) = -\bar{r}(z, \bar{z}) + L(z - \mathrm{i}\bar{r}(z, \bar{z}), \bar{z} + \mathrm{i}r(\bar{z}, z)). \tag{A.32}$$

Expanding this and using (A.29) gives

$$L(z, \bar{z}) = r(z, \bar{z}) + \bar{r}(z, \bar{z}) + \mathrm{i}\psi(z, \bar{z}) + \mathrm{UTs}, \tag{A.33}$$

where

$$\psi(z, \bar{z}) = 2\left(a(z + \bar{z})\bar{r}(z, \bar{z}) - (az + c\bar{z})r(\bar{z}, z)\right). \tag{A.34}$$

Using (A.24) and (A.29), we equate coefficients to get

$$a = 2a_1, \tag{A.35}$$

$$c = 2a_2, \tag{A.36}$$

$$f = 2a_3 - 12a_1b_1 + 4a_2b_2, \tag{A.37}$$

$$g = 2a_4 + 4a_2b_1 + 4a_1b_2. \tag{A.38}$$

The procedure conclusion follows from Theorem 4.3 of [35] using $\mathrm{e}^{\mathrm{i}\phi/2} = \mu = \gamma - \mathrm{i}\sigma$. ∎

Appendix B. Additional details of numerical experiments. Here we provide additional details of the numerical experiments, including the system parameters and the energy drift.

B.1. Experimental system parameters. The flexible water system used in the simulations, equilibrated at either 0.015 K or 300 K, is based upon the TIP3P model [21], with flexibility incorporated by adding bond stretching and angle bending harmonic terms; cf. [23, p. 184]. By equilibrating we avoid highly improbable values of different contributions to energies. Experiments such at those in [8] suggest that flexible water models are particularly sensitive to destabilizing artifacts in numerical integrators. This is a system that has fastest motions with periods of around 10 fs. For each simulation a trace of the following information was generated: all of the components of the energy, positions (trajectories), velocities, and forces.

The potential energy function for an electrostatic interaction is given by

$$U_{ij}^{\text{electrostatic}} = C\frac{q_i q_j}{x_{ij}} SWC1(x_{ij}), \tag{B.1}$$

where $x_{ij} = \|x_j - x_i\|$ is the distance between atoms i and j, q_i is the charge for atom i, and $C = 332.0636\,\text{kcal mol}^{-1}\,\text{K}^{-1}$. Coulomb energies were split into fast and slow multiplying by the following C^1 switching function:

$$C^1(\vec{r}_{ij}) = \begin{cases} 1 - (\frac{3}{2}|\vec{r}_{ij}|{r_1}^2 - \frac{1}{2}|\vec{r}_{ij}|^3){r_1}^{-3} & \text{if } |\vec{r}_{ij}| \le r_1, \\ 0 & \text{if } |\vec{r}_{ij}| > r_1, \end{cases} \tag{B.2}$$

where r_1 is the cutoff distance where the function value becomes zero. The cutoff used for our test system was 6.5 Å.

The energy for a Lennard–Jones interaction is

$$U_{ij}^{\text{Lennard-Jones}} = 4\epsilon_{ij}\left(\left(\frac{\sigma_{ij}}{x_{ij}}\right)^{12} - \left(\frac{\sigma_{ij}}{x_{ij}}\right)^{6}\right) SWC2(x_{ij}), \tag{B.3}$$

where ϵ_{ij} and σ_{ij} are the Lennard–Jones energy minimum and crossover point (where the Lennard–Jones function is zero).

Lennard–Jones energies were split using the following C^2 switching function:

$$C^2(\vec{r}_{ij}) = \begin{cases} 1 & \text{if } |\vec{r}_{ij}| \le r_0, \\ \dfrac{(|\vec{r}_{ij}|^2 - {r_1}^2)^2({r_1}^2 + 2|\vec{r}_{ij}|^2 - 3{r_0}^2)}{({r_1}^2 - {r_0}^2)^3} & \text{if } r_0 \le |\vec{r}_{ij}| < r_1, \\ 0 & \text{if } |\vec{r}_{ij}| > r_1, \end{cases} \tag{B.4}$$

where r_1 is the distance where the function value becomes zero, and r_0 is that where it becomes active. The values in our experiments were 6.5 Å and 0.1 Å, respectively.

The energy for a bond interaction is

$$U_k^{\text{bond}} = \frac{1}{2}K_{\text{B}}(x_{ij} - l_k)^2, \tag{B.5}$$

where K_{B} is a bond force constant and l_k is a reference bond length between atoms i and j for constraint k. Finally, the energy for an angle interaction is

$$U_k^{\text{angle}} = \frac{1}{2}K_{\text{A}}(\theta_k - \theta_0)^2, \tag{B.6}$$

where K_{A} is an angle force constant, and θ_k and θ_0 are the current value of the angle and the reference angle for angle constraint k.

For flexible water, $K_{\text{A}} = 55\,\text{kcal mol}^{-1}\,\text{degrees}^2$, $K_{\text{B}} = 450\,\text{kcal mol}^{-1}\,\text{Å}^2$, $q_{\text{O}} = 0.417\,\text{e}$, $q_{\text{H}} = -0.834\,\text{e}$, $l_{\text{O-H}} = 0.957\,\text{Å}$, and $\theta_0 = 104.52\,\text{degrees}$. The Lennard–Jones parameters are $\sigma_{\text{H-H}} = 0.4\,\text{Å}$, $\sigma_{\text{O-O}} = 3.1506$ Å, $\sigma_{\text{O-H}} = 1.75253\,\text{Å}$, $\epsilon_{\text{H-H}} = 0.046\,\text{kcal mol}^{-1}$, $\epsilon_{\text{O-O}} = 0.1521$ kcal mol^{-1}, $\epsilon_{\text{O-H}} = 0.08365$ kcal mol^{-1}.

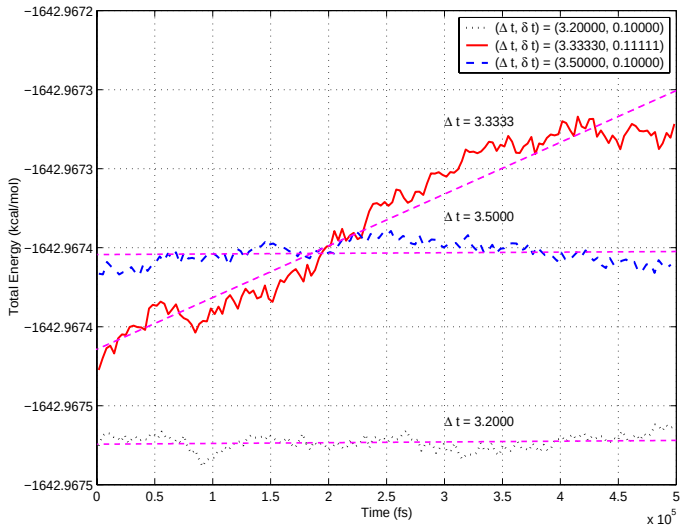

FIG. B.1. *Block-averaged drift of total energy for* 500 *ps of molecular dynamics simulation of 10 Å radius of water using Verlet-I/r-RESPA/Impulse. It illustrates the* 3:1 *nonlinear resonance at a third of the fastest period near zero K. The percent relative drift of total energy of the three simulations is* 0.01%, 0.82%, *and* 0.01% *for* $\Delta t = 3.20\,fs$, $\Delta t = 3.33\,fs$, *and* $\Delta t = 3.50\,fs$, *respectively. The curves have been shifted for clarity with two steps. The curve for* $\Delta t = 3.33\,fs$ *is shifted by* -0.002 kcal/mol *and the curve for* $\Delta t = 3.50\,fs$ *is shifted by* -0.006 kcal/mol. *These negative shifts help to bring the three curves to the same starting point. Then the curve for* $\Delta t = 3.33\,fs$ *is shifted by* 0.00006 kcal/mol *and that for* $\Delta t = 3.50\,fs$ *is shifted by* 0.00012 kcal/mol.

B.2. Detailed view of energy drift. We show the details of the energy drift by plotting the block-averaged energy output to visualize the nonlinear instabilities for simulations at near zero temperature and room temperature; see Figures B.1, B.2, B.3, and B.4. The resonance at a given step size shows itself as an abrupt increase in the drift with respect to neighboring values of the step size. In the absence of resonance the energy would be conserved.

B.3. Flexible water simulation with PME. Simulations of flexible waters presented in Figures 2.2 and 2.3 use the direct method for Coulomb force evaluation and use *vacuum* boundary conditions. We also performed simulations of flexible water using the PME method for Coulomb force evaluation. The 3:1 instability is clearly shown in Figure B.5 at outer step size $\Delta t = 3.27$ fs.

Acknowledgments. We are grateful for the assistance of Thierry Matthey, the lead developer of PROTOMOL. We are also grateful to Dr. Procacci and Dr. Zhou for valuable discussions. We acknowledge the use of the Hydra Unix cluster owned by the College of Engineering of the University of Notre Dame. We also acknowledge the use of the Bob Linux cluster owned by the College of Science and College of Engineering of the University of Notre Dame. We give special thanks to Andrew McCammon and his group at the University of California at San Diego for hosting JI in May, 2001, when discussions that led to this paper took place.

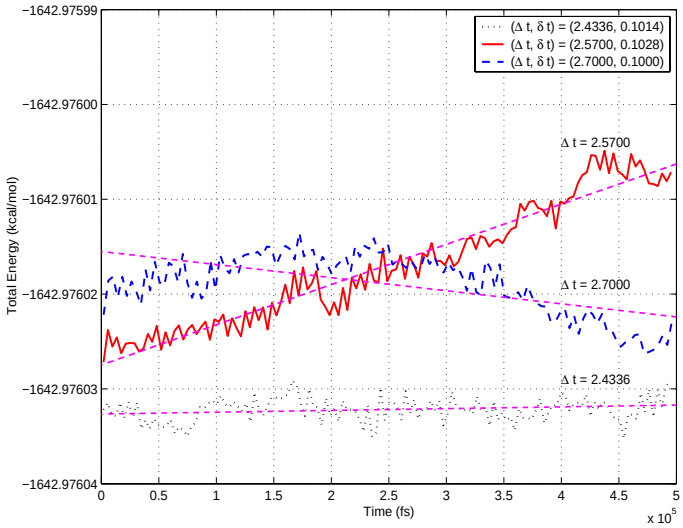

FIG. B.2. *Same as Figure* B.1 *except that it shows evidence of a* 4:1 *nonlinear resonance. The percent relative drift of total energy of the three simulations is* 0.004%, 0.119%, *and* −0.038% *for* $\Delta t = 2.43\,fs$, $\Delta t = 2.57\,fs$, *and* $\Delta t = 2.70\,fs$, *respectively. The curve with* $\Delta t = 2.57\,fs$ *is shifted by* −0.0001 kcal/mol *and the curve with* $\Delta t = 2.70\,fs$ *is shifted by* −0.0021 kcal/mol. *These negative shifts help to bring the three curves to the same starting point. Then, the curve with* $\Delta t = 2.57\,fs$ *is shifted by* 0.000005 kcal/mol *and the curve with* $\Delta t = 2.70\,fs$ *is shifted by* 0.000010 kcal/mol.

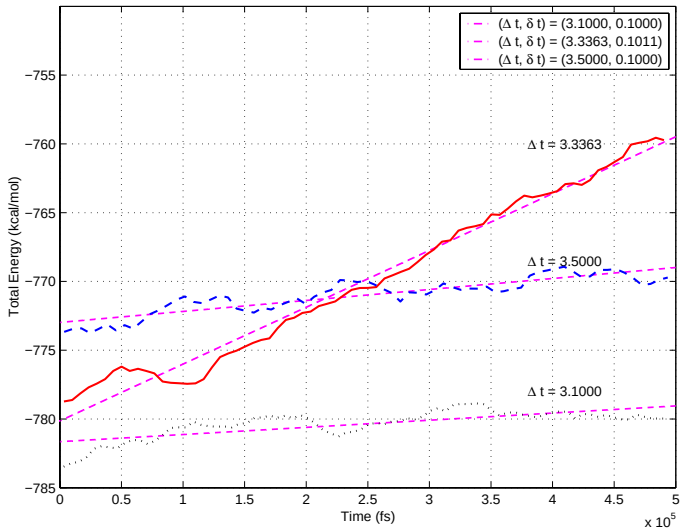

FIG. B.3. *Same as in Figure* B.1 *except that the temperature here is* 300 *K. The percent relative drift of total energy of the three simulations is* 0.70%, 5.42%, *and* 1.07% *for* $\Delta t = 3.10\,fs$, $\Delta t = 3.33\,fs$, *and* $\Delta t = 3.50\,fs$, *respectively. The curves have been shifted for clarity: the curve with* $\Delta t = 3.33\,fs$ *is shifted by* 5.0 kcal/mol *and the curve with* $\Delta t = 3.50\,fs$ *is shifted by* 10.0 kcal/mol. *This shows evidence of the* 3:1 *nonlinear instability due to resonance.*

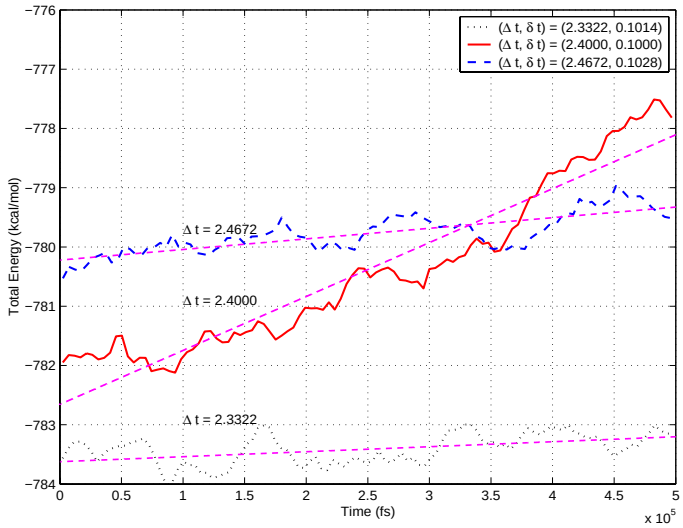

FIG. B.4. *Same as in Figure* B.3 *except that it shows evidence of a possible* 4:1 *resonance. The percent relative drift of total energy of the three simulations is* 0.11%, 1.20%, *and* 0.24% *for* $\Delta t = 2.33\,fs$, $\Delta t = 2.40\,fs$, *and* $\Delta t = 2.47\,fs$, *respectively. The curves have been shifted for clarity: the curve with* $\Delta t = 2.40\,fs$ *is shifted by* 1.5 kcal/mol *and the curve with* $\Delta t = 2.47\,fs$ *is shifted by* 3.0 kcal/mol.

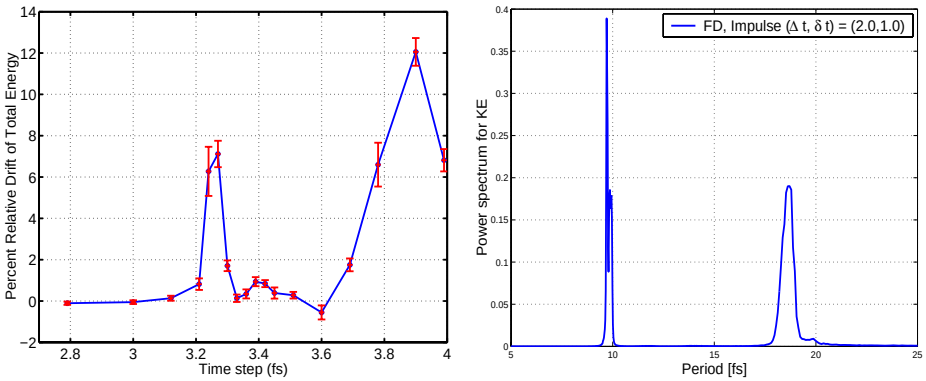

FIG. B.5. *On the left: Same as in Figure* 2.3 *except that the inner step size is* 1/3 *of the outer time step and PME is used in the Coulomb force evaluation.* The peak at step size of 3.27 fs shows 3:1 instability. *On the right: The periods of the fastest normal modes from a* 200 *ps simulation of the same system with inner time step of* 1 *fs at* 300 *K, in which the Coulomb force is evaluated using the direct method.*

REFERENCES

[1] H. C. Andersen, *Rattle: A 'velocity' version of the shake algorithm for molecular dynamics calculations*, J. Comput. Phys., 52 (1983), pp. 24–34.

[2] E. Barth and T. Schlick, *Extrapolation versus impulse in multiple-timestepping schemes* II. *Linear analysis and applications to Newtonian and Langevin dynamics*, J. Chem. Phys., 109 (1998), pp. 1633–1642.

[3] P. F. Batcho, D. A. Case, and T. Schlick, *Optimized particle-mesh Ewald/multiple-time step integration for molecular dynamics simulations*, J. Chem. Phys., 115 (2001), pp. 4003–4018.

[4] P. F. Batcho and T. Schlick, *New splitting formulations for lattice summations*, J. Chem. Phys., 115 (2001), pp. 8312–8326.

[5] P. F. Batcho and T. Schlick, *Special stability advantages of position-verlet over velocity-verlet in multiple-time step integration*, J. Chem. Phys., 115 (2001), pp. 4019–4029.

[6] H. J. C. Berendsen and W. F. van Gunsteren, *Practical algorithms for dynamic simulations*, in Proc. Internat. School of Phys., Enrico Fermi, 97, G. C. Ciccotti and W. G. Hoover, eds., Amsterdam, North–Holland, 1986, pp. 43–65.

[7] J. J. Biesiadecki and R. D. Skeel, *Dangers of multiple-time-step methods*, J. Comput. Phys., 109 (1993), pp. 318–328.

[8] T. Bishop, R. D. Skeel, and K. Schulten, *Difficulties with multiple timestepping and the fast multipole algorithm in molecular dynamics*, J. Comput. Chem., 18 (1997), pp. 1785–1791.

[9] B. García-Archilla, J. M. Sanz-Serna, and R. D. Skeel, *Long-time-step methods for oscillatory differential equations*, SIAM J. Sci. Comput., 20 (1998), pp. 930–963.

[10] B. García-Archilla, J. M. Sanz-Serna, and R. D. Skeel, *The mollified impulse method for oscillatory differential equations*, in Numerical Analysis, D. F. Griffiths and G. A. Watson, eds., London, Pitman, 1998, pp. 111–123.

[11] M. Gribskov, L. Wesson, and D. Eisenberg, *Melittin, the* 2*mlt protein*, Structure available online from http://www.rcsb.org/pdb/ (15 October 1990).

[12] H. Grubmüller, H. Heller, A. Windemuth, and K. Schulten, *Generalized Verlet algorithm for efficient molecular dynamics simulations with long-range interactions*, Molecular Simulation, 6 (1991), pp. 121–142.

[13] E. Hairer, S. P. Nørsett, and G. Wanner, *Solving Ordinary Differential Equations* I: *Non-stiff Systems*, Springer–Verlag, Berlin, 1987.

[14] D. D. Humphreys, R. A. Friesner, and B. J. Berne, *A multiple-time-step molecular dynamics algorithm for macromolecules*, J. Phys. Chem., 98 (1994), pp. 6885–6892.

[15] J. A. Izaguirre, *Longer Time Steps for Molecular Dynamics*, Ph.D. thesis, University of Illinois at Urbana-Champaign, Urbana, IL, 1999.

[16] J. A. Izaguirre, *Generalized mollified multiple time stepping methods for molecular dynamics*, in Multiscale Computational Methods in Chemistry and Physics, NATO Sci. Ser. F Comput. Syst. Sci. 177, A. Brandt, J. Bernholc, and K. Binder, eds., IOS Press, Amsterdam, 2001, pp. 34–47.

[17] J. A. Izaguirre, D. P. Catarello, J. M. Wozniak, and R. D. Skeel, *Langevin stabilization of molecular dynamics*, J. Chem. Phys., 114 (2001), pp. 2090–2098.

[18] J. A. Izaguirre, Q. Ma, T. Matthey, J. Willcock, T. Slabach, B. Moore, and G. Viamontes, *Overcoming instabilities in Verlet-I/r-RESPA with the mollified impulse method*, in Proceedings of 3rd International Workshop on Methods for Macromolecular Modeling, Lect. Notes Comput. Sci. Eng. 24, T. Schlick and H. H. Gan, eds., Springer–Verlag, Berlin, New York, 2002, pp. 146–174.

[19] T. Matthey, T. Cickovski, S. Hampton, A. Ko, Q. Ma, T. Slabach, and J. Izaguirre, *PROTOMOL, an object-oriented framework for prototyping novel applications of molecular dynamics*, ACM Trans. Math. Software, submitted.

[20] J. A. Izaguirre, S. Reich, and R. D. Skeel, *Longer time steps for molecular dynamics*, J. Chem. Phys., 110 (1999), pp. 9853–9864.

[21] W. L. Jorgensen, J. Chandrasekhar, J. D. Madura, R. W. Impey, and M. L. Klein, *Comparison of simple potential functions for simulating liquid water*, J. Chem. Phys., 79 (1983), pp. 926–935.

[22] L. Kalé, R. Skeel, M. Bhandarkar, R. Brunner, A. Gursoy, N. Krawetz, J. Phillips, A. Shinozaki, K. Varadarajan, and K. Schulten, *NAMD2: Greater scalability for parallel molecular dynamics*, J. Comput. Phys., 151 (1999), pp. 283–312.

[23] A. R. Leach, *Molecular Modelling: Principles and Applications*, Addison–Wesley Longman, Reading, MA, 1996.

[24] T. R. Littell, R. D. Skeel, and M. Zhang, *Error analysis of symplectic multiple time*

stepping, SIAM J. Numer. Anal., 34 (1997), pp. 1792–1807.

[25] Q. Ma and J. A. Izaguirre, *Targeted mollified Impulse – A multiscale stochastic integrator for molecular dynamics*, Multiscale Model. Simul., submitted.

[26] Q. Ma and J. A. Izaguirre, *Long time step molecular dynamics using targeted Langevin stabilization*, in Proceedings of the ACM Symposium on Applied Computing, Melbourne, FL, 2003, pp. 178–182

[27] A. D. MacKerell Jr., D. Bashford, M. Bellott, R. L. Dunbrack Jr., J. Evanseck, M. J. Field, S. Fischer, J. Gao, H. Guo, S. Ha, D. Joseph, L. Kuchnir, K. Kuczera, F. T. K. Lau, C. Mattos, S. Michnick, T. Ngo, D. T. Nguyen, B. Prodhom, I. W. E. Reiher, B. Roux, M. Schlenkrich, J. Smith, R. Stote, J. Straub, M. Watanabe, J. Wiorkiewicz-Kuczera, D. Yin, and M. Karplus, *All-hydrogen empirical potential for molecular modeling and dynamics studies of proteins using the CHARMM22 force field*, J. Phys. Chem. B, 102 (1998), pp. 3586–3616.

[28] A. D. MacKerell Jr., D. Bashford, M. Bellott, R. L. Dunbrack Jr., J. Evanseck, M. J. Field, S. Fischer, J. Gao, H. Guo, S. Ha, D. Joseph, L. Kuchnir, K. Kuczera, F. T. K. Lau, C. Mattos, S. Michnick, T. Ngo, D. T. Nguyen, B. Prodhom, B. Roux, M. Schlenkrich, J. Smith, R. Stote, J. Straub, M. Watanabe, J. Wiorkiewicz-Kuczera, D. Yin, and M. Karplus, *Self-consistent parameterization of biomolecules for molecular modeling and condensed phase simulations*, FASEB J., p. 6:A143, 1992.

[29] M. Mandziuk and T. Schlick, *Resonance in the dynamics of chemical systems simulated by the implicit midpoint scheme*, Chem. Phys. Lett., 237 (1995), pp. 525–535.

[30] T. Matthey and J. A. Izaguirre, *ProtoMol: A molecular dynamics framework with incremental parallelization*, in Proceedings of the Tenth SIAM Conference on Parallel Processing for Scientific Computing, Portsmouth, VA, 2001, CD-ROM, SIAM, Philadelphia, PA, 2001.

[31] S. Miyamoto and P. A. Kollman, *SETTLE: An analytical version of the SHAKE and RATTLE algorithm for rigid water molecules*, J. Comput. Chem., 13 (1992), pp. 952–962.

[32] P. Procacci, personal communication, 2002.

[33] P. Procacci and M. Marchi, *Taming the Ewald sum in molecular dynamics simulations of solvated proteins via a multiple time step algorithm*, J. Chem. Phys., 104 (1996), pp. 3003–3012.

[34] P. Procacci, M. Marchi, and G. J. Martyna, *Electrostatic calculations and multiple time scales in molecular dynamics simulation of flexible molecular systems*, J. Chem. Phys., 108 (1998), pp. 8799–8803.

[35] R. D. Skeel and K. Srinivas, *Nonlinear stability analysis of area-preserving integrators*, SIAM J. Numer. Anal., 38 (2000), pp. 129–148.

[36] A. Sandu and T. Schlick, *Masking resonance artifacts in force-splitting methods for biomolecular simulations by extrapolative Langevin dynamics*, J. Comput. Phys, 151 (1999), pp. 74–113.

[37] J. M. Sanz-Serna and M. P. Calvo, *Numerical Hamiltonian Problems*, Chapman and Hall, London, 1994.

[38] T. Schlick, M. Mandziuk, R. D. Skeel, and K. Srinivas, *Nonlinear resonance artifacts in molecular dynamics simulations*, J. Comput. Phys., 139 (1998), pp. 1–29.

[39] R. D. Skeel, *Integration schemes for molecular dynamics and related applications*, in The Graduate Student's Guide to Numerical Analysis, Springer Ser. Comput. Math. 26, M. Ainsworth, J. Levesley, and M. Marletta, eds., Springer–Verlag, Berlin, 1999, pp. 119–176.

[40] R. D. Skeel and J. A. Izaguirre, *The five femtosecond time step barrier*, in Computational Molecular Dynamics: Challenges, Methods, Ideas, Lect. Notes Comput. Sci. Eng. 4, P. Deuflhard, J. Hermans, B. Leimkuhler, A. Mark, S. Reich, and R. D. Skeel, eds., Springer–Verlag, Berlin-Heidelberg-New York, 1998, pp. 303–318.

[41] R. D. Skeel, G. Zhang, and T. Schlick, *A family of symplectic integrators: Stability, accuracy, and molecular dynamics applications*, SIAM J. Sci. Comput., 18 (1997), pp. 203–222.

[42] M. Tuckerman, B. J. Berne, and G. J. Martyna, *Reversible multiple time scale molecular dynamics*, J. Chem. Phys., 97 (1992), pp. 1990–2001.

[43] W. F. van Gunsteren and H. J. C. Berendsen, *Algorithms for macromolecular dynamics and constraint dynamics*, Mol. Phys., 34 (1977), pp. 1311–1327.

[44] R. Zhou and B. J. Berne, *A new molecular dynamics method combining the reference system propagator algorithm with a fast multipole method for simulating proteins and other complex systems*, J. Chem. Phys., 103 (1995), pp. 9444–9459.

[45] R. Zhou, E. Harder, H. Xu, and B. J. Berne, *Efficient multiple time step method for use with ewald and particle mesh ewald for large biomolecular systems*, J. Chem. Phys., 115 (2001), pp. 2348–2358.